metals

MDPI

Article

A Study on the Influence of the Rotating Speed and Load on the Grain Structure and Wear Properties of Bearing Steel GCr15 During Bearing Service

Li Cui [1], Donghui Wang [2], Chenxu Zhang [3] and Xin Wang [1,*]

[1] College of Shipbuilding and Marine Equipment Engineering, Shanghai Polytechnic University, Shanghai 201209, China; cuili@sspu.edu.cn
[2] College of Energy and Materials, Shanghai Polytechnic University, Shanghai 201209, China; wdh13701744275@163.com
[3] Shanghai Vocational and Technical Teacher Education School, Shanghai Polytechnic University, Shanghai 201209, China; chenxu_zhang@126.com
* Correspondence: wangxin2020@126.com; Tel.: +86-(21)5021-8013

Abstract: In order to study the wear failure mechanism and structure evolution law of bearings under different speeds and contact loads, an elastoplastic model of a 7009AC bearing was established in this paper. The stress, temperature rise and grain size during dry friction and wear of the bearing inner ring were simulated with the finite element method. The effects of the inner ring speed, load pressure and other parameters on the wear rate were studied. The relationship between the grain size and yield strength of GCr15 bearing steel was obtained. The effects of the initial grain size, rotational speed and load pressure on the bearing wear failure were studied. The evolutions of the grain size during service were predicted by means of the dynamic grain recrystallization (DRX), static grain recrystallization (SRX) and grain growth (GG) subprogram. The results show that the contact stress has a more significant effect on the early failure wear than the bearing speed, and the increase in the contact stress will aggravate the wear rate of the bearing inner ring. Under the same working conditions, the smaller the grain size, the more significant the influence of the cycle times on wear was. The heat-affected zone produced a local high temperature in the contact area, temperature flashes of up to 580 °C could occur in the central contact area, and the temperature decreased gradually with the increase in the depth from the contact area. It is noteworthy that both the surface and the subsurface of the material produced grain refinement; the grain size was refined from 20 μm to 0.4–12 μm under different working conditions. And the degree of refinement of the subsurface was higher than that of the surface.

Keywords: wear rate; finite element model; friction temperature rise; dynamic recrystallization; grain refinement

check for updates

Citation: Cui, L.; Wang, D.; Zhang, C.; Wang, X. A Study on the Influence of the Rotating Speed and Load on the Grain Structure and Wear Properties of Bearing Steel GCr15 During Bearing Service. *Metals* **2024**, *14*, 1408. https://doi.org/10.3390/met14121408

Academic Editor: Marta Oliveira

Received: 25 October 2024
Revised: 29 November 2024
Accepted: 2 December 2024
Published: 9 December 2024

Copyright: © 2024 by the authors. Licensee MDPI, Basel, Switzerland. This article is an open access article distributed under the terms and conditions of the Creative Commons Attribution (CC BY) license (https://creativecommons.org/licenses/by/4.0/).

1. Introduction

Bearings are usually operated in service under harsh working conditions involving high speeds, heavy loads and high temperatures [1]. Their main failure forms include wear, burns, cracks and spalling [2,3]. The different material characteristics and processing technology of high-speed bearings lead to abnormal state and early wear failure during service. Under harsh conditions, rapid acceleration, collision and high-temperature conditions increase abnormal wear in the contact area, accelerate the failure of the bearing, and aggravate the friction between the bearing rolling element and the raceway [4]. Therefore, in order to improve the service life of bearings and avoid premature bearing wear failure, it is urgent to clarify the influence mechanism of factors such as speed, load and material characteristics on the bearing wear and early failure.

GCr15(AISI-52100) is a typical bearing steel, which has good wear resistance and contact fatigue properties and is widely used in bearing manufacturing [5,6]. Yang et al. proposed a new wear calculation model which was based on the exponential transient volume equation and Archard equation. The predicted value of the wear coefficient is close to the experimental value, but the study did not realize the influence of working conditions on wear [7]. Yin et al. discussed and analyzed the influence of non-uniform load on the performance and wear evolution of cylindrical roller bearings from both the theoretical and experimental aspects, and concluded that non-uniform load could significantly increase the wear and deformation of the bearing raceway surface [8]. Ji et al. studied the effects of load and speed on the friction coefficient and wear under dry friction conditions, and the results showed that speed had a more significant effect on the friction coefficient, while load had a more significant effect on wear [9]. Sander et al. studied the wear mechanism of plain bearings under starting and scram conditions by means of elastic fluid dynamics simulation and obtained the wear depth and contact pressure distribution characteristics of plain bearings under different speed conditions. However, this has not been analyzed and studied according to the law of microstructure evolution [10].

The early wear failure of bearings is not only affected by the service conditions, but also related to the microstructure of the bearing steel [11–13]. The evolution behavior of the grain during service is highly dependent on deformation parameters, including the strain, strain rate, temperature, etc. The evolution of grains includes dynamic recrystallization (DRX), elemental dynamic recrystallization (MDRX) and static recrystallization (SRX) [14–16]. Yin and Hua et al. simulated and studied the microstructure evolution of GCr15 by physical experiments and the finite element method and established the constitutive equations of austenite grain growth and dynamic recrystallization of bearing steel using the linear regression method. However, the effect of the micro grain size on bearing failure was not considered in this paper [17]. Chen et al. completed the finite element analysis of the microstructure evolution of the dynamic recrystallization in the thermal deformation process by establishing the thermoforming finite element model of GCr15 material. However, the influence of grain evolution on the wear failure of bearing products in the service process has not been analyzed [18]. Qin et al. explored the microstructure of high-nitrogen bearing steel X30CrMoN15-1 before rolling contact fatigue and explained the reason for the excellent resistance of the alloy to white corrosion cracking [19]. M.Y. Toumi et al. simulated the surface wear and spalling process of thrust ball bearings under cyclic load using the finite element method, but they did not study the change law of the microstructure in this process [20].

To sum up, the above studies provide the characteristics of microstructure evolution and wear failure mechanisms of different materials. However, in terms of the influence of the microscopic grain size on properties, a large number of studies are only in the research stage of microstructure evolution during the material preparation process, and few studies have considered the friction and wear properties of the initial bearing steel microstructure under different rotation speeds and contact loads and their microstructure evolution rules. Therefore, it is urgent to systematically study the friction and wear mechanism and the evolution of the structure induced by the working conditions and other factors during the service of high-speed ball bearings.

In this paper, the Hall–Petch relation is optimized by the linear regression method and the wear failure depth of high-speed ball bearings is calculated based on the classical Archard model. It is found that the influence of contact stress on the early failure wear of the bearing is more significant than that of the bearing speed, and the increase in the contact stress will aggravate the wear rate of the bearing inner ring. The effects of the speed, radial load and grain size on the friction and wear behavior of high-speed ball bearings were studied. The temperature rises and microstructure evolution of the raceway of bearing inner rings under different working conditions were calculated using the finite element model and verified by corresponding experiments. And the result shows that the finer the grain is under the same working conditions, the more significant the effect of the number of cycles, N, on the wear. The contact area will produce a local high temperature. Under

the coupling effect of temperature and stress, the grain size in the bearing contact region is refined and grown. In addition, there is no relevant modified factor fitting is carried out for the numerical model of grain evolution in this research; the finite element simulation is carried out with the commercial numerical program Deform V11.0, and verified by the experiments in this paper. It is found that the finite element simulation has authenticity and realizability, which provides the basis and conditions for the subsequent study of correction factors and the effect of temperature on grain evolution.

2. Numerical Simulation and Experiment

2.1. Finite Element Geometry and Material Models

In this paper, the common finite element software Deform V11.0 was used to simulate the dry friction process between a bearing inner ring and a type-7009AC (NSK, Shanghai, China) roller. Figure 1 shows the established finite element model. In order to simplify the model and calculation amount, the calculation of stresses and corresponding deformation at a contact point between rolling elements and raceways employs elasticity relations established by Hertz in 1881. Hertz's theory considers the contact of two bodies with curved surfaces under force [21] and the contact between each rolling element and the inner and outer raceway during the running contact of the bearing is called Hertz contact. The study object is simulated according to the Hertz contact theory. The inner diameter of the inner ring model is 45 mm, the pitch circle diameter is 60 mm, the inner ring channel radius is 3.711 mm, and the roller diameter is 7.136 mm. The lower surface of the inner ring is fixed. Rollers rotate at 2000 rpm and 12,000 rpm, respectively, and the contact area is equipped with 1000 MPa, 1500 MPa and 2000 MPa contact loads, respectively.

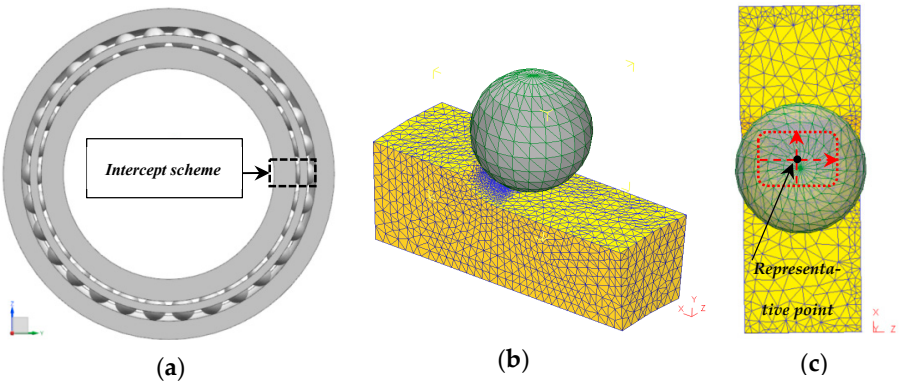


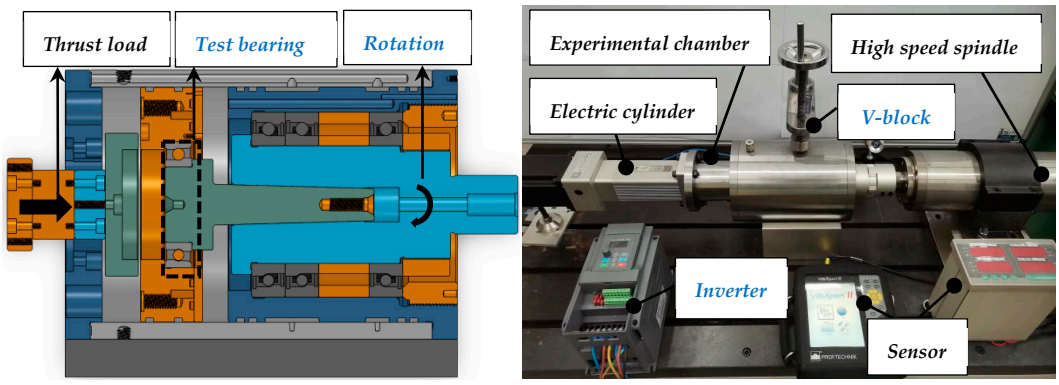
Figure 1. 7009AC bearing geometry model: (**a**) geometrical model of bearing; (**b**) simplified finite element model; (**c**) model representativeness analysis position.

The purpose of this paper is to study the wear failure and precision loss of the raceway of the bearing inner ring, so the inner ring can be set as the plastic body and the roller can be set as the analytic rigid body, and the analytical rigid body in the finite element software Deform V11.0 does not require meshing. The model was divided into tetrahedral grids and the contact area was refined. The grids of rollers and inner rings are shown in the figure below. The total number of grids in the model was 26,377. The initial model temperature setting is the same as room temperature, here, set to 20 °C. The inner ring model set the initial grain size to 20 μm.

In the process of bearing service, the microscopic grains of the material evolve in the form of dynamic recrystallization (DRX), static recrystallization (SRD) and austenite grain growth (GG). The temperature field, stress field and strain field during rolling friction can be calculated using the finite element model, and the relationship between the grain size and the variables of these fields can be established. Therefore, in this paper, the DRX, SRD and GG constitutive models of GCr15 embedded in Deform V11.0 are used to predict the microscopic grain evolution process.

2.2. Experimental Materials and Methods

Experimental material was selected as NSK for the bearing inner ring of the 7009AC model. The material type is bearing steel GCr15 (as shown in Figure 2). The cylindrical roller material is GCr15 after vacuum quenching, and the hardness range is HRC55-HRC58. The material composition [17] is shown in Table 1.



(**a**) (**b**)

Figure 2. Experimental schematic diagram and device: (**a**) schematic diagram of the experimental chamber; (**b**) experimental facility.

Table 1. Element content of GCr15/%.

Materials	C	Mn	Si	Cr	Ni	Mo	S	P	V	N	Fe
521,000	0.96	0.36	0.19	1.46	0.08	0.02	0.006	0.01	/	/	Bal.

The contact angle of the test inner ring is 25°, the pitch circle diameter is 60 mm and the number of balls is 21. The width is 16 mm. The finite element model is consistent with the size of the inner ring test specimen, and the diameter of the test roller is 7.136 mm. In the durability test, the contact stress of the bearing surface will also exceed 3.4 GPa [22], and considering that the yield strength of the selected bearing material is 2.1 GPa, the experimental contact sum is selected as 2 GPa. At the same time, considering the running performance of the experimental device, the bearing speed is set as 2000 rpm in the experiment to achieve the low-speed and heavy-load working conditions. Therefore, a speed of 2000 rpm and a load of 2 GPa are applied to the experimental bearing to change the number of loading cycles to accelerate the wear failure.

The friction test was carried out with the bearing wear experimental device designed in the laboratory, as shown in Figure 2b. The device consists of a drive shaft, a coupling, a bearing wear test device, an axial loading device, a water-cooling system and a control cabinet. Before the experiment, the test bearing was ultrasonically cleaned 3 times in the ultrasonic cleaning machine (KQ3200DE, Kunshan ultrasonic instrument Co., Ltd., Kunshan, China) for 120 min each and the lubricating oil inside the test bearing was removed. About 0.1 ml of lubricating oil was added to make the bearing in an inadequate state of lubrication to accelerate bearing wear.

In the course of the experiment, considering the use efficiency of the experimental instrument, the experimental efficiency and the accuracy of the experimental verification, three sets of tests were carried out with a contact load of 2000 rpm and 2000 MPa given the input shaft speed. The initial state of the test bearing is used for comparison, and the loading experiment is not carried out. After a rolling cycle under inadequate lubrication conditions, the inner ring sample is removed from the testing machine and the wear results are measured. The distribution of elements and the microscopic changes on the worn surface were observed with a scanning electron microscope (SEM, JSM-6610LV,

JEOL, Shanghai, China) and energy dispersive spectrometer (EDS, Ultim Max 65, Oxford Instruments, Shanghai, China). The disk was sliced from the center of the track, then ground, polished and etched with 5% nitric acid to observe the deformation microstructure under the worn surface. The microscopic grain size at the specified location was measured to verify the simulation results. The microstructure under the worn surface was studied by X-ray diffraction (XRD, Oxford C-nano, D8 Advance, BRUKER, Shanghai, China).

3. Results and Discussion

3.1. Hall–Petch Relationship and Grain Size Growth Model

As mentioned above, grain size plays an important role in the mechanical properties of materials. The Hall–Petch relationship between the yield strength and initial grain size is calculated by the finite element model. According to the Hall–Petch relation (see Formula (1) [23]), grain refinement can improve the strength of polycrystalline materials, where Y_S is the yield strength, δ_0 is the stress when the dislocation moves on the slip plane, which can also be understood as the yield strength of a single crystal, d is the average grain size, and k is the influence coefficient of the grain boundary on the strength, which is a constant value.

$$Ys = \delta_0 + kd^{-\frac{1}{2}} \quad (1)$$

The empirical formula shows that within a certain grain size range, which is from 4 μm to 20 μm, the finer the grain size, the higher the strength of the polycrystalline material [24].

Figure 3 shows the fitting curve of the Hall–Petch relationship between the grain size and yield strength of GCr15 bearing steel. The fitting relationship between the grain size and yield strength of bearing steel is as follows:

$$Ys = 1696.95 + 1161/\sqrt{d} \quad (2)$$

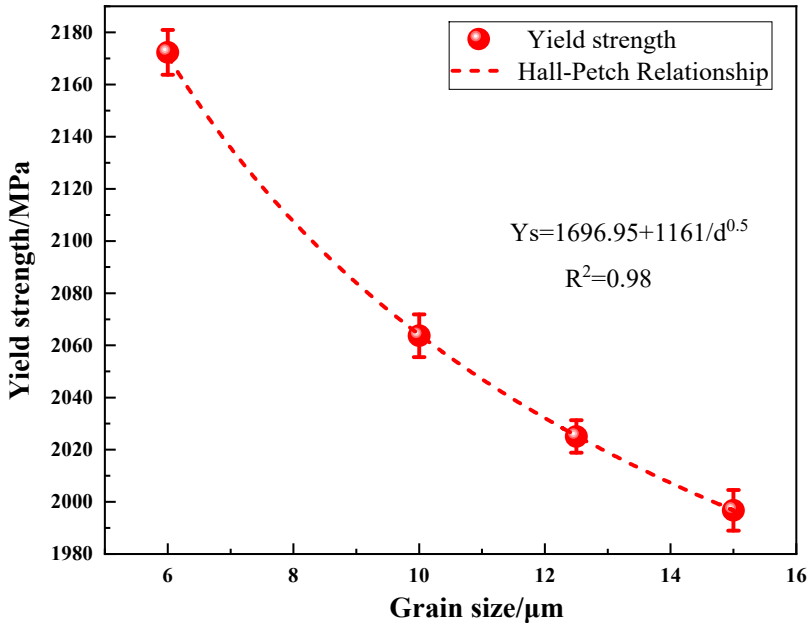


Figure 3. Hall–Petch fitting relationship of GCr15.

The goodness of fit R^2 is 0.98. Because the grain boundary free energy is higher than the inner cell free energy, grain refining increases the grain boundary density in the material, thereby increasing the barrier of dislocation slip and ultimately improving the strength of the material.

The essence of the Hall–Petch relation is the numerical representation of the fine grain strengthening theory. According to the formula, the threshold value of the microstructure

characteristics can be determined under the specified required strength. For GCr15, when the yield strength is not less than 2.1 GPa, the upper threshold of the grain size of bearing steel GCr15 is 8.29 μm.

The microstructure in the metastable state is formed after the recrystallization process of the material, and the microstructure has internal energy for grain evolution at this time. In order to obtain a more stable structure and release the internal potential of the grain, the grain will continue to grow after recrystallization, the grain size will increase, and the grain boundary area per unit volume will decrease. The grain growth of C-Mn steel can be represented by the following model [17]:

$$d^n = d_0^n + Atexp\left(-\frac{Q}{RT}\right) \tag{3}$$

In the above formula, d is the grain size after growth, d_0 is the initial grain size, t is the isothermal holding time, Q is the activation energy of crystal growth, R is the constant value of gas 8.314 J/mol·K, T is the temperature in the contact zone, in Kelvin (K), and A, n is the material constant.

Regarding the austenite grain growth model, Yada et al. proposed the classic austenite grain growth model of carbon steel, in which the constants and parameters are as follows: [25]

$$d^2 = d_0^2 + 1.44 \times 10^{12} texp\left(-\frac{26700}{RT}\right) \tag{4}$$

The theoretical model described above has been programmed in the commercial software Deform V11.0 by computer language, so it can be used directly and simulated numerically.

3.2. Influence of Contact Stress and Rotational Speed on Bearing Wear Rate

The bearing surface stress will change significantly during service. Different stress changes have a significant influence on bearing failure. In this section, the surface stress of a 7009AC-model inner ring under different working conditions is simulated by Deform. The bearing wear rate changes under six working conditions at 2000 rpm and 12,000 rpm and contact loads of 1000 MPa, 1500 MPa and 2000 MPa were calculated and analyzed by the Archard model. Figure 4 shows the influence of contact stress and speed on the wear rate of the bearing inner ring. The cycles of P4 precision wear failure of GCr15 with contact loads of 1 GPa, 1.5 GPa and 2 GPa at 2000 rpm at different initial grain sizes are given.

It can be seen from Figure 4 that with the increase in the grain size, the number of wear failure cycles of bearing steel gradually decreases. When the initial grain of GCr15 is small, the larger the contact load at the bearing contact point is, the smaller the number of cycles that can be served. When the rotation speed is 2000 rpm, the maximum number of cycles occurs when the contact load is 1 GPa. When the initial grain size is not less than 10 μm, the increase in the grain size has little effect on the number of wear failure cycles of GCr15. It can be seen from Figure 4a that the influence of different contact loads on the number of cycles is greater than that of different rotational speeds. This may be because the increase in load is more likely to increase the temperature of the friction surface [26]. Due to the influence of various factors such as a high temperature and working conditions, the impact of load on the wear rate is greater than that of the rotating speed. When the contact load increases to 1.5 GPa and 2 GPa, respectively, the number of bearing wear failure cycles decreases by about 2 × 104 and 3 × 104 times. It has also been confirmed that with the increase in the contact load, the number of cycles of bearing wear failure is reduced. With the increase in the bearing load, the frictional contact area increases, thus reducing the wear failure life [27].

Figure 4b–d show the influence of speed on the ball bearing wear failure. The wear failure cycles at 2000 rpm and 12,000 rpm were compared under different contact loads. The analysis shows that when the contact load is constant, with the increase in the bearing speed, the wear rate will accelerate [28], and the number of wear failure cycles of the

bearing will decrease. In addition, with the increase in the grain size, the number of bearing wear cycles decreases. This indicates that for polycrystalline materials, the grain refinement of bearings during friction has an important effect on their hardness, and the hardness of GCr15 decreases with the increase in grain size [29]. That is, as the grain size increases, the hardness of the material decreases, resulting in less wear resistance and fewer cycles. The number of cycles decreased rapidly in the 4–8 μm region. When the grain size is greater than 8 μm and the contact load is 1 GPa, the slope of the decline curve of wear failure cycles of high and low speed bearings decreases from 0.2 and 0.19 to 0.06 and 0.05, respectively, with the increase in the grain size. This indicates that the decline rate of the bearing wear failure cycles slows down with the increase in the grain size in the large grain region. The presence of local dislocation clusters in fine grains may lead to a sharp increase in bearing strength with the decrease in the grain size. That is, with the increase in the grain size, the change in the material strength of the large grain material is smaller than that of the fine grain material [30].

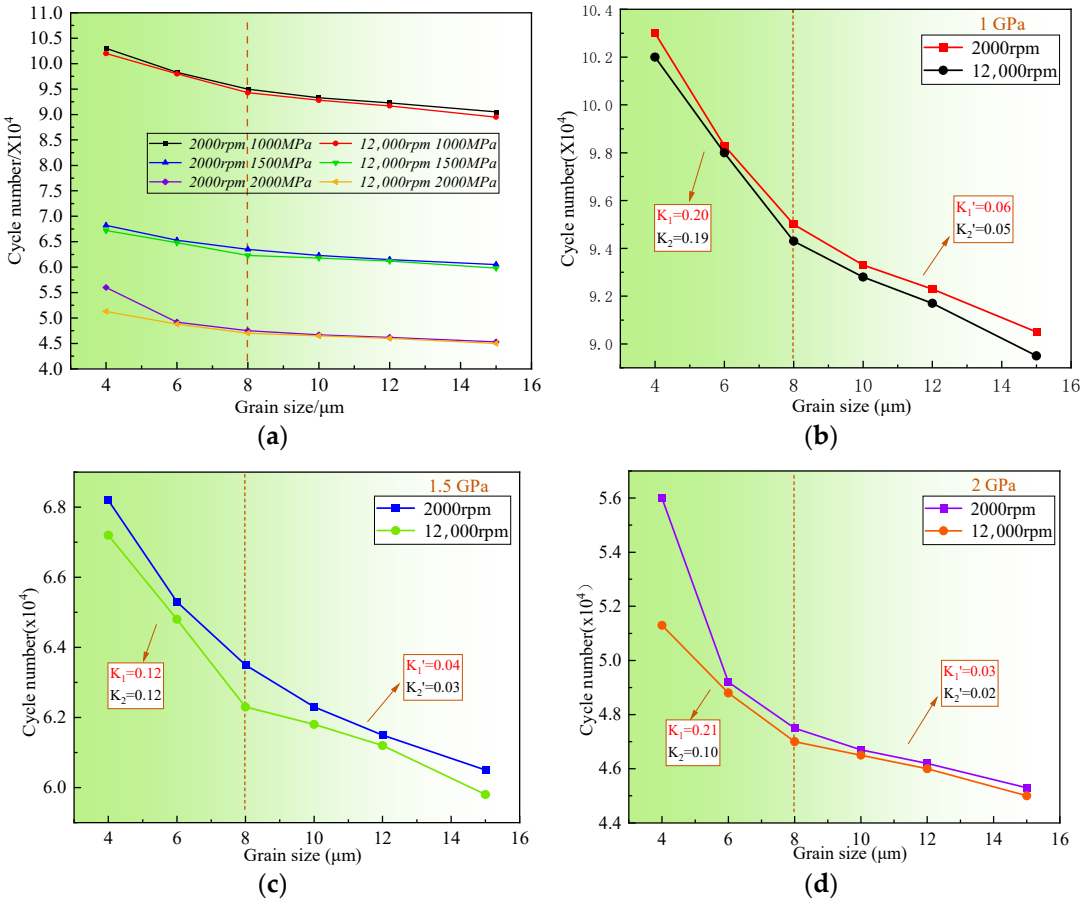


Figure 4. Influence of contact load and speed of GCr15 on the number of cycles (wear rate): (**a**) effect of bearing contact load; (**b**) effect of speed under 1 GPa; (**c**) effect of speed under 1.5 GPa; (**d**) effect of speed under 2 GPa.

3.3. Influence of Contact Stress and Rotational Speed on Surface Temperature

In this section, the temperature simulation of a 7009AC model inner ring and cylindrical roller bearing model is carried out by Deform software. The temperature variation under different conditions of contact stress and rotational speed is simulated. The initial temperature of the model was set to room temperature, 24 °C. The main form of heat dissipation in the temperature simulation in this paper is heat transfer between the inner ring and the roller. In order to study more deeply the influence of load and speed on the temperature rise in the contact area during the bearing service, this section analyzes the

temperature change law of the bearing inner ring after 200 min of dry friction activity under speeds of 2000 rpm and 12,000 rpm and working conditions of 1000 MPa, 1500 MPa and 2000 MPa under four different initial grain sizes. The influence of the experimental parameters on the temperature variation in the friction contact area of the bearing is obtained.

Figure 5 shows the typical temperature distribution at the contact point between the bearing roller and the inner ring at 12,000 rpm and 2000 MPa during the bearing service. The temperature distribution and situation under other working conditions have similar morphological characteristics associated with them. Since the rolling friction between the bearing roller and the inner ring only occurs in the Hertzian contact area [31], a large temperature rise is generated only in the contact area, and the temperature rise occurs in the adjacent position through heat conduction and heat radiation. After mutual rolling and friction between the roller and the inner ring, the temperature of the contact area of the inner ring surface is the highest, at about 580 °C, and the subsurface temperature decreases with the increase in the depth from the surface. In addition, the temperature changes in other areas of the inner ring that are farther from the contact area are small. That is, only the near-contact region has a large temperature gradient, while the internal region has a small temperature gradient. This is due to the fact that the temperature in the loaded area of the bearing is higher than in the unloaded area during service, and the highest temperature is located in the direction parallel to the load [32].

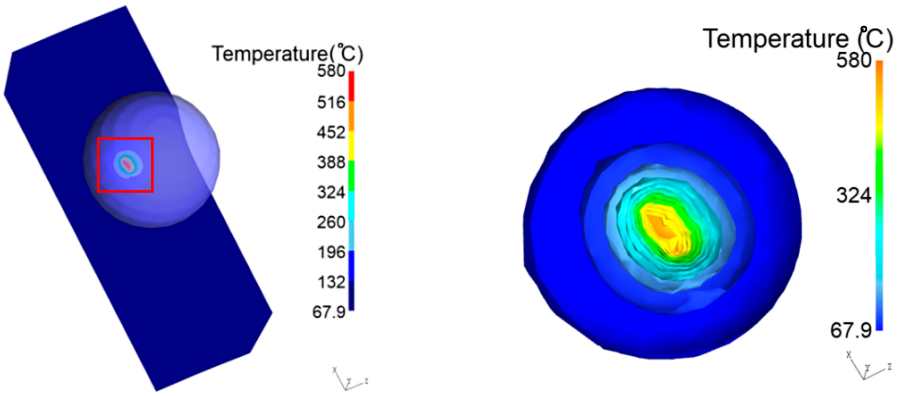


Figure 5. Temperature distribution of the bearing under 12,000 rpm and 2000 MPa working conditions: (**a**) 3D morphology; (**b**) the contact influence zone.

During the entire bearing friction and wear process, the temperature rise process will also change due to the different loading conditions and speeds. In order to characterize the temperature rise process under different service conditions, the temperature changes in the inner ring contact position under different working conditions were tracked and are plotted in Figure 6. With the rolling friction, the temperature in the bearing contact area tends to rise. This indicates that the heat generated by friction in the rolling contact areas during bearing service is greater than the heat dissipation in these areas, and the heat gradually accumulates and rises [33]. It can be seen from analyzing Figure 6 that, in the friction process of bearings with insufficient lubrication, when the initial grain is the same, the temperature rise trend in the contact region has the same characteristics under different speeds and contact loads. Figure 6a shows the temperature variation trend of the inner ring contact area after 200 min of dry sliding friction at 2000 rpm and 1000 MPa. It can be concluded that the temperature flicker occurs in the dry friction stage of the bearing [33]. The maximum flash temperature is 478 °C. Figure 6b shows the temperature variation trend of the inner ring contact area after 200 min of dry sliding friction at 12,000 rpm and 1000 MPa. The temperature variation trend under other working conditions is shown in Figure 6c–f. With the increase in the rotational speed, the temperature flashover frequency

and temperature in the contact area increase. As can be seen from Figure 6, when the pressure is constant, the frequency of temperature flashovers in the contact area advances with the increase in the rotational speed.

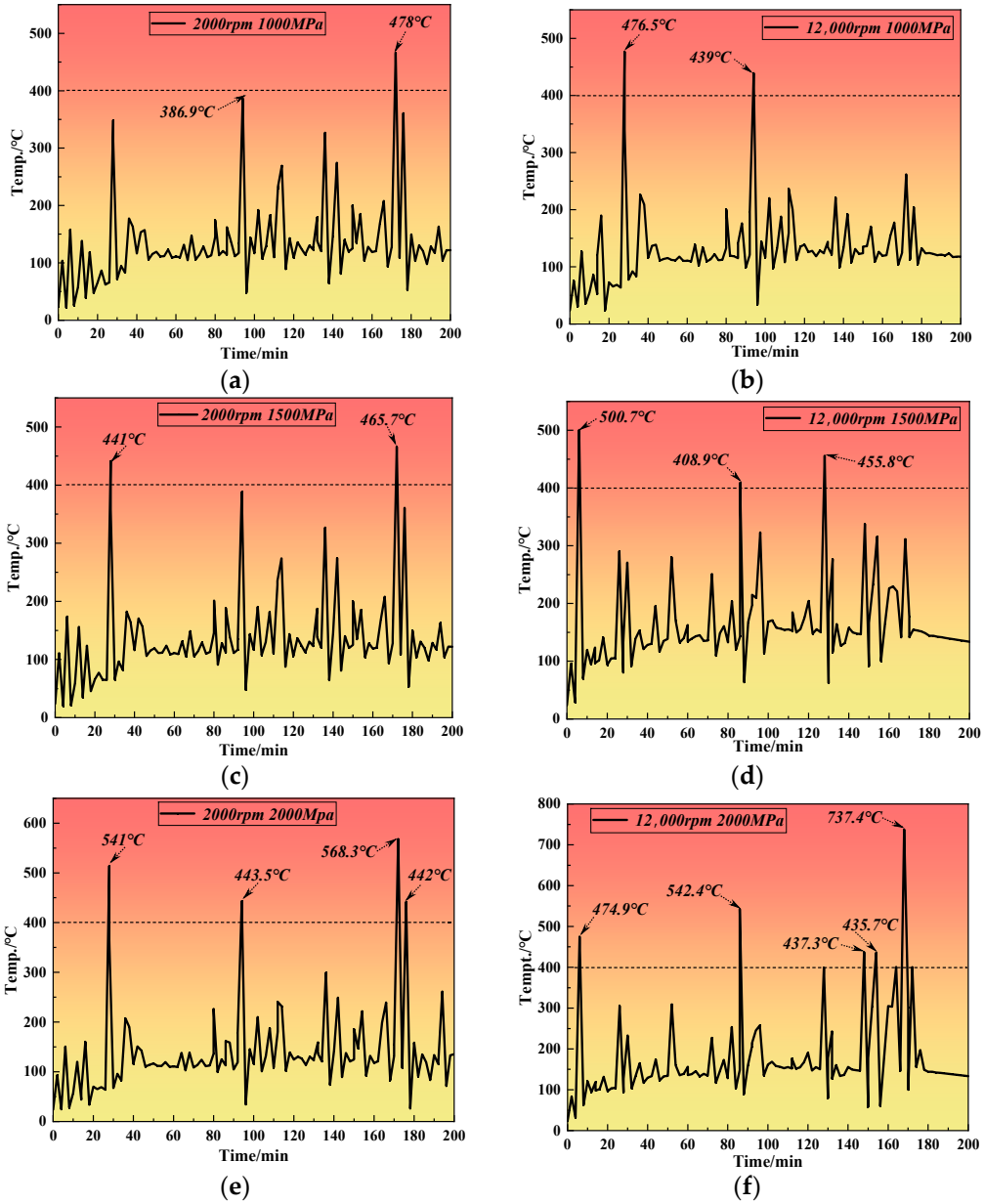


Figure 6. GCr15 contact area temperature variation trend under different working conditions: (**a**) 2000 rpm, 1000 MPa; (**b**) 2000 rpm, 1500 MPa; (**c**) 2000 rpm, 2000 MPa; (**d**) 12,000 rpm, 1000 MPa; (**e**) 12,000 rpm, 1500 MPa; (**f**) 12,000 rpm, 2000 MPa.

When the rotational speed is constant, the temperature rise in the contact area increases gradually with the increase in the load. When the load is constant, the temperature rise in the contact area gradually increases with the increase in the rotational speed [34]. It can be noticed that, at the same speed, the temperature rise caused by the increase in the contact load increases more than that caused by the increase in speed, which means that dry friction causes a larger temperature rise by increasing the pressure than by increasing the speed with the other conditions kept the same. When the contact load increases, the contact area of the friction pair increases, which leads to a more obvious temperature rise [35].

3.4. Influence of Contact Stress and Rotational Speed on Microscopic Grains

Under the experimental conditions of dry friction, the contact area will produce a rapid temperature rise, accompanied by changes in the microstructure. For GCr15, considering the initial microscopic average grain size, the grain change trend during the service process was simulated at 2000 rpm and 12,000 rpm speeds and contact loads of 1000 MPa, 1500 MPa and 2000 MPa. The grain evolution process caused by the rolling friction between the roller and the inner ring during the bearing's service is simulated by the grain size calculation program of the finite element software. Considering the initial microcosmic average grain size of the material, the grain variation trend during its service was simulated.

It can be seen from the simulation results in Figure 7 that the grain size in the raceway contact area is small, and the grain size in other areas of the raceway does not evolve. The results show that the grain refinement of the contact region increases with the increase in the rotational speed and contact load when other conditions are kept the same [36].

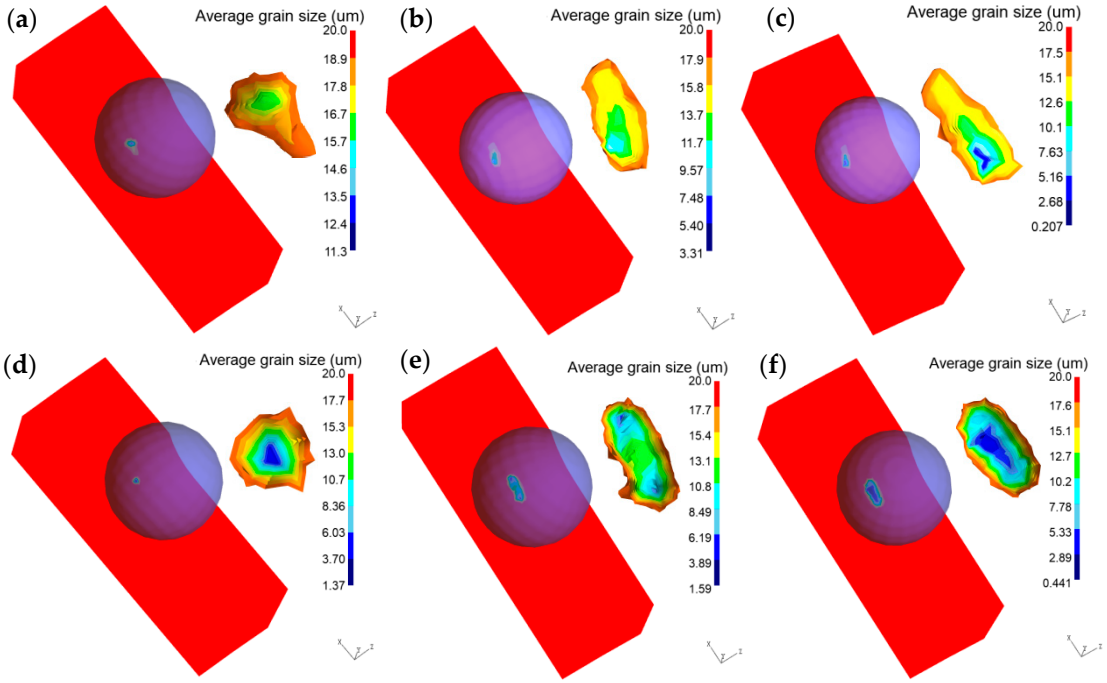


Figure 7. Grain distributions of GCr15 under different working conditions. (**a**) 2000 rpm, 1000 MPa; (**b**) 2000 rpm, 1500 MPa; (**c**) 2000 rpm, 2000 MPa; (**d**) 12,000 rpm, 1000 MP; (**e**) 12,000 rpm, 1500 MP; (**f**) 12,000 rpm, 2000 MPa.

In addition, as shown in Figure 7, the simulation results show that the grain refinement regions all present a common feature of approximately elliptical regions. This is consistent with the Hertz contact theory when the bearing roller is in contact with the inner ring. This means that the microstructure refinement mechanism of the friction layer in the contact area of the bearing inner ring is caused by the strong coupling effect of stress and friction heat.

Figure 8 plots the evolution curve of the grain size on the surface of the contact area with strain during the rolling friction between the bearing roller and the inner ring. It can be seen that the micro grain size of the bearing will change with the increase in the strain variable during service. Under the same working conditions, with the increase in the strain variable, the micro grain size of the bearing decreases first and then increases. This change trend is consistent with the recrystallization trend of the contact area during bearing service [37].

Figure 9 shows the effect of the grain size evolution on the wear rate when the initial grain size is 20 μm. It can be seen from the figure that during the service of the bearing, the grains in the contact area will be refined and recrystallized. With the increase in the number

of cycles, the refined grains will continue to grow. The grain sizes at different stages are different, which will have different effects on the early wear failure of the bearing. It can be concluded from the figure that the wear rate of the bearing is relatively significant in the initial service stage, which shows macroscopic performance in the running-in stage. When the friction cycle lasts for a certain period of time, it enters the stable wear stage. At this time, the grain refinement plays a role in reducing the wear rate of the bearing. This is due to the increased interaction force between the bearing microscopic grain boundaries during service, which improves the wear resistance of the raceway [38], but the wear rate will reach 100% with the increase in the cycle times.

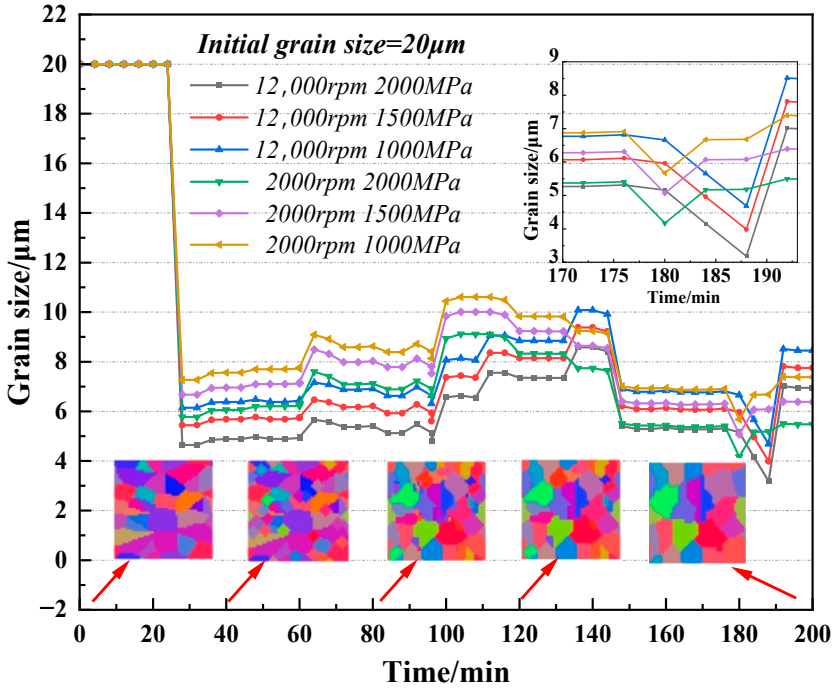


Figure 8. Grain evolution of the bearing inner ring at an initial grain size of 20 μm.

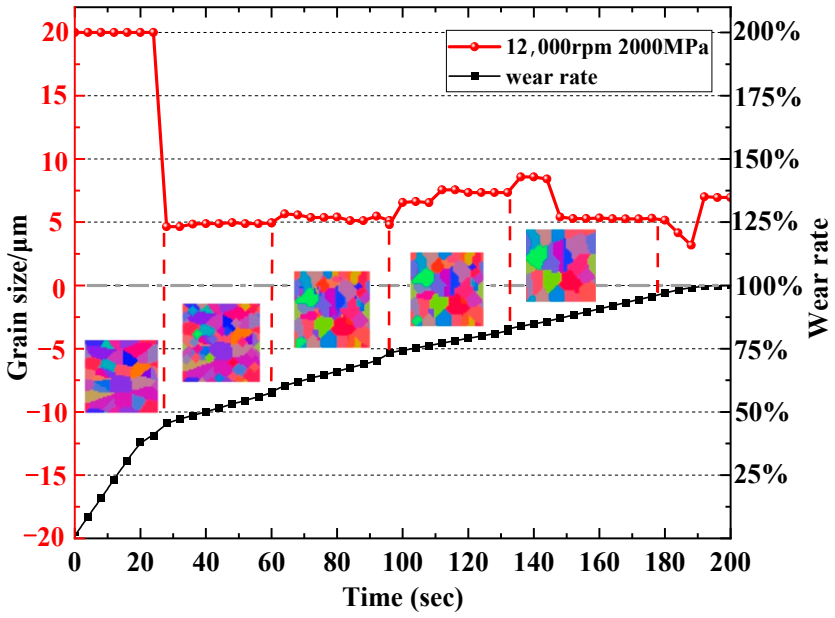
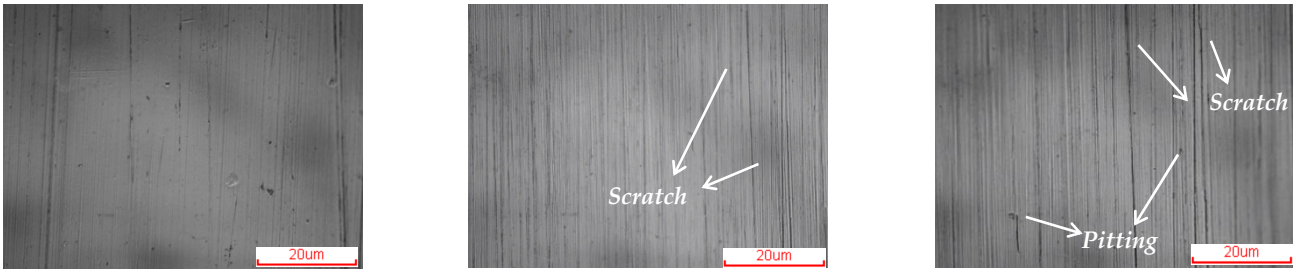


Figure 9. Effect of grain evolution on wear rate at an initial grain size of 20 μm.

3.5. Friction Surface Wear Analysis

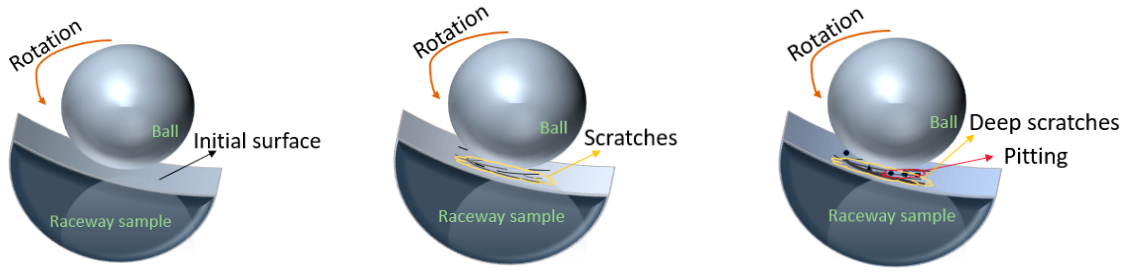
In order to explain the surface wear of the bearing inner ring at 2000 rpm and 2000 MPa, Figure 10 shows the surface wear diagram of the bearing inner ring at different speeds. The surface topography of the initial inner ring was compared with the surface topography of the bearing inner ring contact area after 2.5 × 106 and 5 × 106 service times. Specifically, when the load is the same as the speed, the surface wear of the contact area gradually increases with the increase in the number of cycles. Different degrees of grooving and spalling appeared in the contact area of the two samples. For the sample after cycling 5 × 106 times, the surface wear and the number of furrows in the contact area gradually increased, and slight pitting points appeared on the contact surface.



(**a**) (**b**) (**c**)

Figure 10. OM with different numbers of cycles: (**a**) original sample surface; (**b**) 2.5 × 106 times; (**c**) 5 × 106 times.

The main damage forms of friction surfaces include scratches, furrows, surface pitting and a small amount of abrasive wear and adhesive wear. In the process of intense friction of the material due to contact pressure and impact, a small number of metal particles fall off and first appear on its surface, freely participating in friction between the friction surfaces [39]. Figure 11 shows the wear mechanism in different periods of the dry friction stage, which are the initial stage, the mid-wear stage and the state model at the end of the tests. The wear debris is affected by friction and load, and participates in the formation of the adhesive on the friction surface. In addition, the pressure and impact act on the brittle and hard adhesive metal at the same time and produce cracks, which eventually leads to the exfoliation of the surface material and the pitting corrosion [40].



(**a**) (**b**) (**c**)

Figure 11. Wear modes and mechanisms during the dry sliding wear test. (**a**) Original sample surface; (**b**) after a period of wear and tear; (**c**) end of wear test.

3.6. Microstructural Characterization

Figure 12 shows the SEM and EDS of the contact area section of the test bearing after 2.5 × 10^6 and 5 × 10^6 cycles at 2000 rpm and 2000 MPa. It can be seen from Figure 12a that the color distribution of the radial section in the SEM of the bearing sample in the initial stage is uniform; that is, the grain size is uniform. The comparative analysis in Figure 12b,c shows that two differently colored regions of light and dark distribution can be observed

in the section of the GCr15 bearing. This indicates that grain refinement occurs on the surface and subsurface of the bearing during its service [41], and the grain density per unit area increases. This is consistent with the grain refinement simulation results and grain variation trends in Section 3.4.

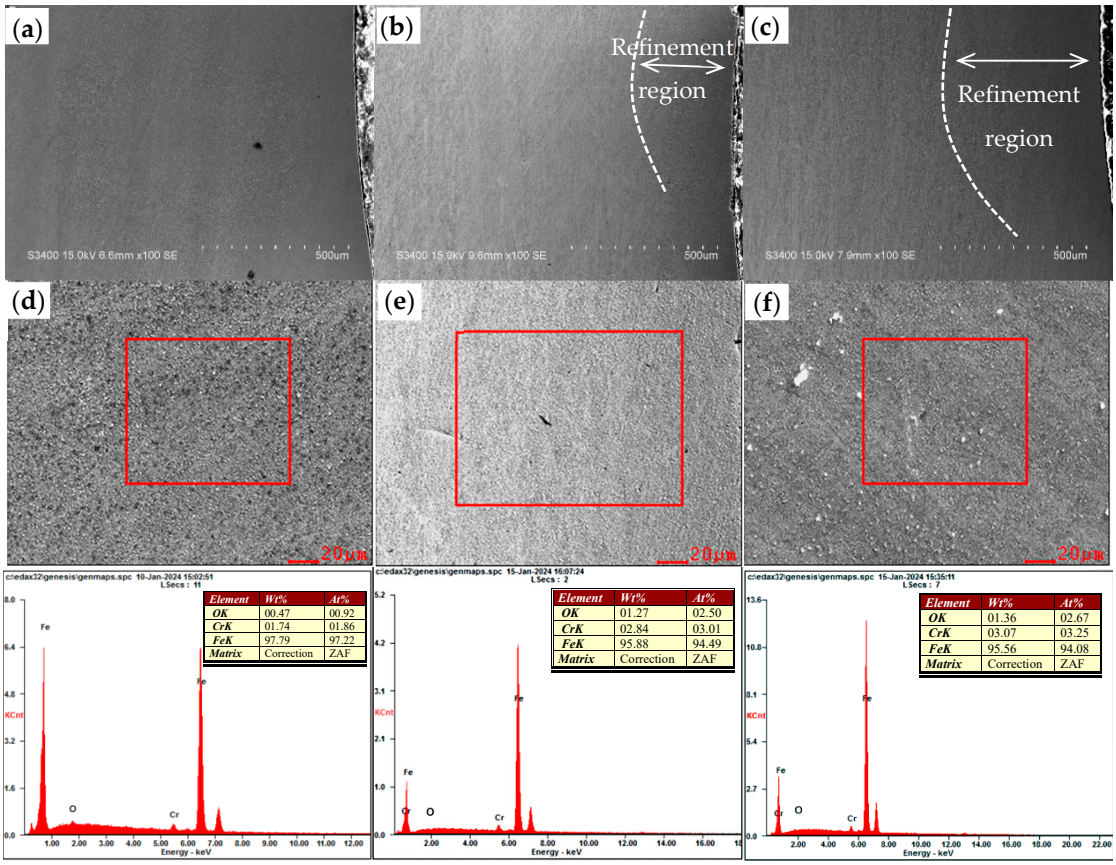


Figure 12. SEM and EDS with different numbers of cycles. (**a**) Initial sample surface; (**b**) Sample surface of 2.5 × 10^6 cycles; (**c**) Sample surface of 5 × 10^6 cycles; (**d**) Initial EDS detection; (**e**) EDS detection of 2.5 × 10^6 cycles; (**f**) EDS detection of 5 × 10^6 cycles.

Figure 12d–f show the EDS of the sample surface of the bearing sample under the working conditions of 2000 rpm and 2000 MPa with different numbers of cycles. It can be seen from Figure 12d–f that, in the initial state of the bearing, the surface of the contact area is smooth and flat. The EDS analysis shows that in the initial state, the worn surface is rich in Fe, Cr and O, and the proportion of O atoms is 0.92%, indicating that the surface is covered with a stable oxide film at this time. When the contact area is cycled 2.5 × 106 and 5 × 106 times, respectively, the main elements on the bearing surface are still Fe, Cr and O. However, the proportion of O atoms on the surface increases from 2.5% to 2.67%, which indicates that the surface oxide film increases. In addition, wear debris and small cracks appear on the bearing sample contact surface. This may be due to the fact that, when the bearing is under heavy load conditions, the oxide film continues to break and form, the oxide film formation rate is lower than the failure rate, and it causes adhesive wear [42].

The evolution of the volume fraction of martensite and austenite in bearing materials under different cycle times was analyzed by XRD, and the influence of cycle times on the phase transformation of martensite and austenite was revealed. The results are shown in Figure 13. As the number of cycles increases, the intensity of the martensite diffraction peaks increases, while the intensity of the austenite diffraction peaks decreases; this indicates that martensitic transformation occurred during the bearing service. The increase in the martensite diffraction peak intensity indicates that the content of martensite in the material

increases [43]. Martensitic phase transformation strengthening ensures the stability of bearing materials during their service to a certain extent.

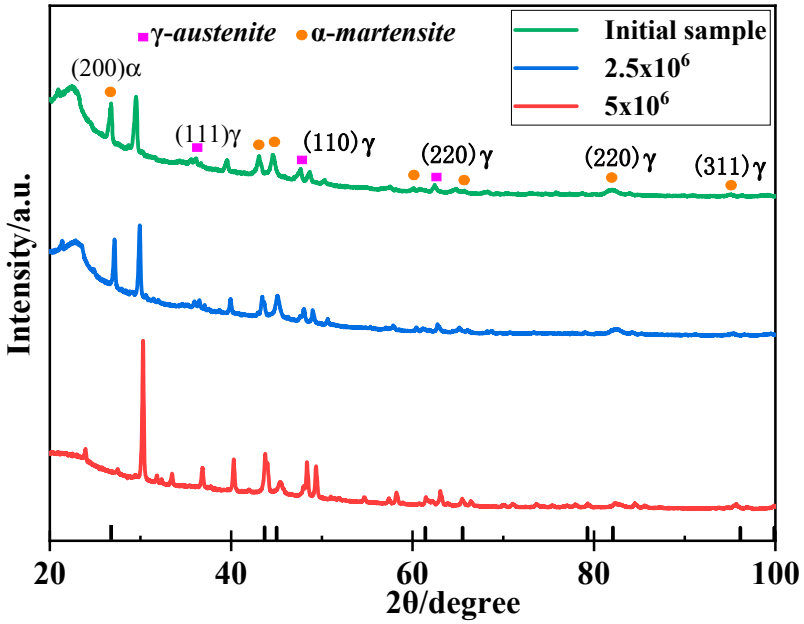


Figure 13. XRD patterns with different numbers of cycles.

4. Conclusions

Research on the wear behavior of high-speed ball bearings during service has produced the following conclusions:

(1) A thermodynamic coupled finite element model of the dry friction process of ball bearings is established, which can model the inner ring wear process under different initial grain sizes. The prediction of the grain size evolution process in the bearing service dry friction process is realized.

(2) In the bearing during its service process, there is an obvious Hall–Petch relationship between the microstructure and the mechanical properties of the material, and the relationship between the grain size and the yield strength is

$$Ys = 1696.95 + 1161/\sqrt{d} \quad (5)$$

(3) In the bearing service process, the contact stress has a more significant impact on the early failure wear than the bearing speed. When the contact load is increased from 1 GPa to 1.5 GPa and 2 GPa, respectively, the number of cycles decreases faster than when the speed is increased from 2000 rpm to 12,000 rpm. The increase in the contact stress will aggravate the wear of the bearing inner ring, accelerate the fatigue failure of the bearing, and reduce the retention time of the bearing rotation accuracy. The number of cycles in the bearing contact area to maintain the P4 accuracy is significantly reduced.

(4) When the grain size is greater than 4 and less than 8 μm, the number of bearing cycles increases greatly with the decrease in the grain size. When the grain size is greater than 8 μm, the number of cycles N of wear failure changes less with the change in the grain size; that is, the finer the grain is under the same working conditions, the more significant the effect of the number of cycles, N, on the wear.

(5) In the bearing service process, the contact area will produce a local high temperature. Under the coupling effect of temperature and stress, the grain in the bearing contact area is refined and grows. At 12,000 rpm and 200 MPa, the average grain size of GCr15 is refined from 20 μm to about 5 μm and then slowly grows to 9 μm,

accompanied by grain size refinement again. The subsurface grain growth rate in the contact region is lower than that of the surface, resulting in the subsurface grain size being larger than the surface grain size.

(6) The grain evolution of the bearing inner ring under different rotational speeds and contact loads was studied. Refined grains were produced on the subsurface, and the grain density increased, which was thought to be related to the increase in the dislocation density in the early subsurface crack initiation of the bearing.

(7) The temperature variation rule of bearings in the friction process has been studied, and the influence of temperature on the results is not considered. However, the mechanism of the influence of temperature on the grain and wear results in the service process of bearings is still unclear, and the author will continue to study this in subsequent research.

Author Contributions: L.C.: conceptualization, methodology, investigation, writing—original draft preparation, writing—review and editing, supervision; D.W.: conceptualization, software, validation, investigation, writing—original draft preparation, project administration; C.Z.: formal analysis, resources, data curation; X.W.: Writing—review and editing, visualization, funding acquisition. All authors have read and agreed to the published version of the manuscript.

Funding: This research was funded by [Shanghai Natural Science Foundation] grant number [20ZR1421000].

Data Availability Statement: The original contributions presented in this study are included in the article. Further inquiries can be directed to the corresponding author.

Conflicts of Interest: The authors declare no conflict of interest.

References

1. Xu, F.; Ding, N.; Li, N.; Liu, L.; Hou, N.; Xu, N.; Guo, W.; Tian, L.; Xu, H.; Wu, C.-M.L.; et al. A review of bearing failure Modes, mechanisms and causes. *Eng. Fail. Anal.* **2023**, *152*, 107518. [CrossRef]
2. Yin, H.; Wu, Y.; Liu, D.; Zhang, P.; Zhang, G.; Fu, H. Rolling Contact Fatigue-Related Microstructural Alterations in Bearing Steels: A Brief Review. *Metals* **2022**, *12*, 910. [CrossRef]
3. Arakere, N.K. Gigacycle rolling contact fatigue of bearing steels: A review. *Int. J. Fatigue* **2016**, *93*, 238–249. [CrossRef]
4. Dhanola, A.; Garg, H.C. Tribological challenges and advancements in wind turbine bearings: A review. *Eng. Fail. Anal.* **2020**, *118*, 104885. [CrossRef]
5. Lorenz, S.J.; Sadeghi, F.; Trivedi, H.K.; Kirsch, M.S. Investigation into rolling contact fatigue performance of aerospace bearing steels. *Int. J. Fatigue* **2023**, *172*, 107646. [CrossRef]
6. Bhadeshia, H.K.D.H. Steels for bearings. *Prog. Mater. Sci.* **2012**, *57*, 268–435. [CrossRef]
7. Yang, L.J. Wear coefficient equation for aluminium-based matrix composites against steel disc. *Wear* **2003**, *255*, 579–592. [CrossRef]
8. Yin, X.; Gu, H.; Feng, G. Analysis of non-uniform abrasion evolution for cylindrical roller bearings. *Mech. Mach. Theory* **2017**, *117*, 148–159. [CrossRef]
9. Ji, C.Y.; Jin, X.Y.; Chen, Z.P. Analysis on tribological properties and contact stress during friction process of sic ceramic materials. *Lubr. Eng.* **2018**, *43*, 78–81.
10. Sander, D.E.; Allmaier, H. Starting and stopping behavior of worn journal bearings. *Tribol. Int.* **2018**, *127*, 478–488. [CrossRef]
11. Li, J.; Liu, J. Strain Compensation Constitutive Model and Parameter Optimization for Nb-Contained 316LN. *Metals* **2019**, *9*, 212. [CrossRef]
12. Ma, Z.-m.; Zhu, H.; Cao, Y.-b.; Yang, S.-p. Evolution of microstructure and mechanical properties of the high-speed train bearing under different service periods. *Mater. Sci. Eng. A* **2021**, *800*, 140345. [CrossRef]
13. Gu, C.; Wang, M.; Bao, Y.; Wang, F.; Lian, J. Quantitative Analysis of Inclusion Engineering on the Fatigue Property Improvement of Bearing Steel. *Metals* **2019**, *9*, 476. [CrossRef]
14. Huang, K.; Logé, R.E. A review of dynamic recrystallization phenomena in metallic materials. *Mater. Des.* **2016**, *111*, 548–574. [CrossRef]
15. Dang, L.; Yang, H.; Guo, L.-g.; Shi, L.; Zhang, J.; Zheng, W.-d. DRX rules during extrusion process of large-scale thick-walled Inconel 625 pipe by FE method. *Trans. Nonferrous Met. Soc. China* **2015**, *25*, 3037–3047. [CrossRef]
16. Han, H.; Zhao, X.; Ding, H.; Zhang, C.; Yu, X.; Wang, W. Numerical Simulation of Microstructure Evolution of Large GCr15 Bar during Multi-Pass Rough Rolling. *Metals* **2022**, *12*, 812. [CrossRef]
17. Yin, F.; Hua, L.; Mao, H.; Han, X.; Qian, D.; Zhang, R. Microstructural modeling and simulation for GCr15 steel during elevated temperature deformation. *Mater. Des.* **2014**, *55*, 560–573. [CrossRef]
18. Chen, X.; Sun, J.; Yang, Y.; Liu, B.; Si, Y.; Zhou, J. Finite Element Analysis of Dynamic Recrystallization Model and Microstructural Evolution for GCr15 Bearing Steel Warm–Hot Deformation Process. *Materials* **2023**, *16*, 4806. [CrossRef]

19. Qin, Y.; Li, J.; Herbig, M. Microstructural origin of the outstanding durability of the high nitrogen bearing steel X30CrMoN15-1. *Mater. Charact.* **2020**, *159*, 110049. [CrossRef]
20. Toumi, M.Y.; Murer, S.; Bogard, F.; Bolaers, F. Numerical simulation and experimental comparison of flaw evolution on a bearing raceway: Case of thrust ball bearing. *J. Comput. Des. Eng.* **2018**, *5*, 427–434. [CrossRef]
21. García-León, R.A.; Martínez-Trinidad, J.; Campos-Silva, I.; Figueroa-López, U.; Guevara-Morales, A. Wear maps of borided AISI 316L steel under ball-on-flat dry sliding conditions. *Mater. Lett.* **2021**, *282*, 128842. [CrossRef]
22. Harris, T.A.; Kotzalas, M.N. *Advance Concept of Bearing Technology: Rolling Bearing Analysis*, 5th ed.; CRC Press: Boca Raton, FL, USA, 2007.
23. Hansen, N. Hall–Petch relation and boundary strengthening. *Scr. Mater.* **2004**, *51*, 801–806. [CrossRef]
24. Ghodrati, M.; Ahmadian, M.; Mirzaeifar, R. Modeling of rolling contact fatigue in rails at the microstructural level. *Wear* **2018**, *406–407*, 205–217. [CrossRef]
25. Yada, H. Prediction of microstructural changes and mechanical properties in hot strip rolling. In Proceedings of the Metallurgical Society of the Canadian Institute of Mining and Metallurgy; Ruddle, G.E., Crawley, A.F., Eds.; Elsevier: Amsterdam, The Netherlands, 1988; pp. 105–119.
26. Phtl, H.; Tosun, N. Effect of load and speed on the wear behavior of woven glass fabrics and aramid fibre-reinforced composites. *Wear* **2002**, *252*, 979–984.
27. Wang, H.; Liu, Z.; Zou, L.; Yang, J. Influence of both friction and wear on the vibration of marine water lubricated rubber bearing. *Wear* **2017**, *376*, 920–930. [CrossRef]
28. Liangjie, M.; Mingjie, C.; Guorong, W. Effect of rotation speed on the abrasive–erosive–corrosive wear of steel pipes against steel casings used in drilling for petroleum. *Wear* **2018**, *410*, 1–10.
29. Pawlak, K.; Białobrzeska, B.; Konat, Ł. The influence of austenitizing temperature on prior austenite grain size and resistance to abrasion wear of selected low-alloy boron steel. *Arch. Civ. Mech. Eng.* **2016**, *16*, 913–926. [CrossRef]
30. Wang, Z.; Baker, I.; Guo, W.; Poplawsky, J.D. The effect of carbon on the microstructures, mechanical properties, and deformation mechanisms of thermo-mechanically treated Fe40.4Ni11.3Mn34.8Al7.5Cr6 high entropy alloys. *Acta Mater.* **2017**, *126*, 346–360. [CrossRef]
31. Golmohammadi, Z.; Sadeghi, F.; Walvekar, A.; Saei, M.; Mistry, K.K.; Kang, Y.S. Experimental and analytical investigation of effects of refurbishing on rolling contact fatigue. *Wear* **2017**, *392*, 190–201. [CrossRef]
32. Liu, M.; Zhou, W.; Song, H.; Dong, Y.; Wang, W.; Zhou, S. Study of the temperature distribution of a machine tool spindle bearing based on FBG quasi-distributed sensing. *Int. J. Adv. Manuf. Technol.* **2018**, *98*, 263–274. [CrossRef]
33. Ju, F.D.; Huang, J.H. Heat checking in the contact zone of a bearing seal (a two-dimensional model of a single moving asperity). *Wear* **1982**, *79*, 107–118. [CrossRef]
34. Jiang, W.; Wang, W.; Ma, M. Study on the flash temperature phenomenon in the contact area of rolling bearings. *Ind. Lubr. Tribol.* **2023**, *75*, 981–992. [CrossRef]
35. Zhang, C.; Zhang, T.; Li, X.; Lv, Y.; Zhong, B. Effect on friction performance of mining wet brake under different working conditions. *Mech. Adv. Mater. Struct.* **2021**, *28*, 27–42. [CrossRef]
36. Guo, R.; Lei, X.; Zhang, D.; Liu, Z.; Wang, X.; Wei, Y. Case Study: The effect of running distance on the microstructure and properties of railroad axle bearings. *Wear* **2017**, *394*, 159–165. [CrossRef]
37. Nikolic, K.; Ferreira, V.M.; Malet, L.; Depover, T.; Verbeken, K.; Petrov, R.H. Uncovering the white etching area and crack formation mechanism in bearing steel. *Mater. Charact.* **2023**, *197*, 112659. [CrossRef]
38. Rai, P.K.; Shekhar, S.; Mondal, K. Effects of grain size gradients on the fretting wear of a specially-processed low carbon steel against AISI E52100 bearing steel. *Wear* **2018**, *412/413*, 1–13. [CrossRef]
39. Anoopnath, P.R.; Babu, V.S.; Vishwanath, A.K. Hertz Contact Stress of Deep Groove Ball Bearing. *Mater. Today Proc.* **2018**, *5*, 3283–3288. [CrossRef]
40. García-León, R.A.; Martínez-Trinidad, J.; Zepeda-Bautista, R.; Campos-Silva, I.; Guevara-Morales, A.; Martínez-Londoño, J.; Barbosa-Saldaña, J. Dry sliding wear test on borided AISI 316L stainless steel under ball-on-flat configuration: A statistical analysis. *Tribol. Int.* **2021**, *157*, 106885. [CrossRef]
41. Wang, Y.-B.; Li, S.-X.; Lu, S.-Y.; Cao, J. New microstructure of butterfly white etching area in rolling contact fatigue of bearing steel. *Tribol. Int.* **2023**, *188*, 108811. [CrossRef]
42. Chen, F.; Wang, B.; Cao, Z. Microstructure and Wear Behavior of In Situ ZA27/TiB2 Composites. *Metals* **2020**, *10*, 1663. [CrossRef]
43. Liu, S.; Li, W.; Shen, J.; Yang, X.; Wang, B.; Liu, J. Size-dependent constitutive model incorporating grain refinement and martensitic transformation. *Arch. Civ. Mech. Eng.* **2023**, *23*, 38. [CrossRef]

Disclaimer/Publisher's Note: The statements, opinions and data contained in all publications are solely those of the individual author(s) and contributor(s) and not of MDPI and/or the editor(s). MDPI and/or the editor(s) disclaim responsibility for any injury to people or property resulting from any ideas, methods, instructions or products referred to in the content.